Eur. Phys. J. Plus (2025) 140:429
https://doi.org/10.1140/epjp/s13360-025-06152-z

THE EUROPEAN PHYSICAL JOURNAL PLUS

Regular Article

Synchrotron-based transmitted, Compton and fluorescence photons from phantom materials

D. V. Rao[1,a], **G. E. Gigante**[1], **R. Cesareo**[2], **A. Brunetti**[2], **N. Schiavon**[3], **T. Akatsuka**[4], **T. Yuasa**[4], **T. Takeda**[5]

[1] Physics Division, Department of Science Based Applications to Engineering (SBAI), University of Rome "La Sapienza", Via Scarpa 10, 00161 Rome, Italy
[2] Istituto di Matematica e Fisica, Università di Sassari, Via Vienna 2, 07100 Sassari, Italy
[3] Hercules Laboratory, University of Evora, Evora, Portugal
[4] Department of Bio-System Engineering, Faculty of Engineering, Yamagata University, Yonezawa-shi, Yamagata 992-8510, Japan
[5] Allied Health Science, Kitasato University, 1-15-1 Kitasato, Sagamihara, Kanagawa 228-8555, Japan

Received: 1 December 2024 / Accepted: 18 February 2025

Abstract Synchrotron-based transmitted, Compton and fluorescence photons from phantom materials composed of light elements, for example, Water, PMMA, Polyethylene, Bakelite, Muscle and Bone, are evaluated, using 10, 15, 20, 30 and 40 keV synchrotron X-rays. The SYRMEP beam line facility at Elettra is used as a source of X-rays. The present research is focused to assess the contribution of transmitted, Compton and fluorescence photons, for the above materials with a test phantom of small dimensions with simple approximations. The phantom structures are composed of light elements or mainly tissue substitutes routinely used to simulate radiation interactions in the human body or test objects. To standardize the image parameters, simple mechanical phantoms are designed. The total number of photons in the bounded area, fluorescent photons, interacted Compton photons, Compton photons for a given solid angle and the number of Compton photons detected at 90° are assessed, for the above phantom materials.

1 Introduction

When X-rays interact with matter, there are three primary interaction modes, i.e., photoelectric effect, Compton and Rayleigh scattering. In first approximation, Rayleigh scattering can also refer to elastic scattering in the X-ray regime (often also referred as Thomson scattering) which is almost constant with respect to energy and atomic number, covering 5–10% of the total effects, and Compton effect is important, especially at high X-ray energies and for low Z elements. Majority of the test phantoms used in the field of medicine are composed of light elements, which constitutes the soft tissue and considerable percentage of the interactions in tissues are scattering. Extensive and critically evaluated reviews on photon interactions in medical and biological context [1–4], tabulations of photon mass energy transfer and mass energy-absorption coefficients [5, 6] and new applications in 'keV' region [7] are reported in the literature. These studies motivated us further to work with the use of synchrotron X-rays. Usually, the measured signal corresponds to transmitted radiation, i.e., the fraction of the initial radiation not interacting with the sample. This is the case, for example, in mammographic, radiographic and tomographic measurements. In all these cases, the photons not interacting with the sample and reaching the detector carry useful information, from the sample. The transmitted and fluorescence contributions also contain useful information, and these positive properties have been studied utilizing synchrotron X-rays.

New tomographic methods were extensively used for the detection of fluorescent X-rays, materials analysis, art and archeometry, and these methods also cover differential and Compton tomography, with tube source of X-rays [8–11]. Photon scattering, with tube source of X-rays, provided new source of information in medicine and biology and material discrimination [12–16]. There are numerous situations in which a convenient and tunable source of monochromatic X-rays would be desired. The flux emitted by the X-ray tube is considerably less and reduces the required monochromacy. An ideal monochromatic radiation comes from a synchrotron source and assessment using synchrotron radiation will be a good choice.

Most of the test phantom materials composed of light elements such as H, C, N, O, P and Ca constitute the soft tissue. The present test phantoms materials of medical interest contain varying compositions of these elements in the atomic region $1 \leq Z \leq 20$. We have chosen the energy region, to assess the individual contribution of transmitted, Compton and fluorescence photons. Further, to estimate the ratio of transmited, Compton and fluorescence contributions, to reflect on contrast, in image-based experiments. The contrast improvement in various imaging techniques mainly depends on low-contrast phantoms used as test objects. In recent years, tomographic imaging, based on scattered radiation from few materials, provides a potential source of information utilizing the

[a] e-mail: done9venkat53@rediffmail.com (corresponding author)

Published online: 21 May 2025

monochromatic X-rays [17–20]. These earlier studies were limited to one material, focused on tomographic imaging-based scattered radiation. Based on the experimental evidence, we extended the study for the other materials, to assess the transmission, Compton and fluorescence photons, in a small volume element. The measured signal corresponds to transmitted radiation, i.e., the fraction of initial radiation not interacting the sample. It reflects on mammographic, radiographic and tomographic measurements. The present experimental data provide useful information and arise from a few phantom materials of biological and medical context. In view of above, it is interesting to investigate the photons when irradiating a small volume element with a source of monochromatic radiation.

2 Materials and methods

We have chosen tunable monochromatic X-rays in the energy range 8–40 keV. The SYRMEP beam line facility at Elettra is used instead of conventional tube source of X-rays. SYRMEP beamline is the first bending magnet of section n. 6 of ELETTRA (beamline 6.1). The horizontal acceptance covered by the front-end light-port is 7 mrad. The beamline provides, at a distance of about 23 m from the source, a monochromatic, laminar section X-ray beam with a maximum area of about 160×5 mm^2. The optics is based on a double-crystal Si (111) monochromator which works in an energy range between 8 and 40 keV. The beamline provides at a distance of about 20 m from the source, a monochromatic or white, laminar section X-ray beam with a maximum area of 120×4 mm^2. The horizontal acceptance covered by the light-port of the front-end is 7 mrad.

With this system, any beam dimensions ranging from a few μm^2 to the maximum beam cross-section are thus made available in the experimental hutch. Downstream of the slit system, and immediately upstream from the sample, a large area, nitrogen-flushed, custom built ionization chamber read out by a Keithley amperemeter is used to monitor the incoming beam and thus to evaluate the dose delivered to the samples.

The influence of the geometrical factor on some of these reference materials on Compton profile measurements has been extensively studied. The same reference materials have been used in the present study, and full details are mentioned [21].

2.1 Experimental procedure

Experimental arrangement used in the present study for the detection of the scattered radiation, reflection geometry, physical dimensions of some of the samples and the electronics associated with Si-PIN detector are shown in Fig. 1a–d.

The scattered radiation from the sample in the energy region 10–40 keV is detected using a Si-PIN detector. The detector is fixed in horizontal plane at an angle of 90° to the incident beam, and the distance between sample and detector is 10 cm. The choice of 90° geometry between the incident beam and detector allowed to reduce the inelastically scattered background (Compton scattering). In this way, the background is reduced considerably, and the fluorescent signal is detected efficiently. The effective solid angle photon beam is determined by a set of collimators. The scattered radiation is detected from a very small volume element, i.e., at the intersection of the collimated source and detector. The output of the Si-PIN detector is coupled to a multi-channel analyzer. It is detecting the transmitted, fluorescence and Compton photons from the sample placed at a distance of 10 cm. Samples of PMMA, Polyethylene and Bakelite, which were prepared as homogeneous cylinder samples, and samples for Water, Muscle and Bone were prepared by placing or pouring in cylinder-shaped sample containers. This data collection procedure was repeated three times to give a total acquisition time of 10^3 s.

2.2 Simple approximations

2.2.1 Estimation of Compton scattered photons in transmission and reflection mode, i.e., at 45°

The number of photons entered at A, i.e., along the line AC (inset, Fig. 2a), is estimated using the following parameters: $N_0 = 10^8$, $(\mu/\rho) = i$ (i = attenuation coefficient of the sample) and t = 5 mm (thickness of small volume element). With the use of these values, the total number of photons entered at A, and the number of fluorescence photons detected at 90° arrived at B with inclusion of 1% of iodine to water is evaluated. The difference gives the interaction of the photons with in the area bounded by ABCD, and the number of photons interact due to Compton process is estimated using Eq. (1) [22–25].

$$N_c = N_{(A-B)}\left[\frac{\mu_{cw}}{\mu_t} * 0.99 + \frac{\mu_{cI}}{\mu_t} * 0.01\right] \tag{1}$$

where μ_{cw} is the Compton coefficient of water, μ_{cI} is the Compton coefficient of iodine and μ_t is the total attenuation coefficient at the incident photon energy. The number of Compton photons detected in a solid angle, and the maximum attenuation at 90° was obtained.

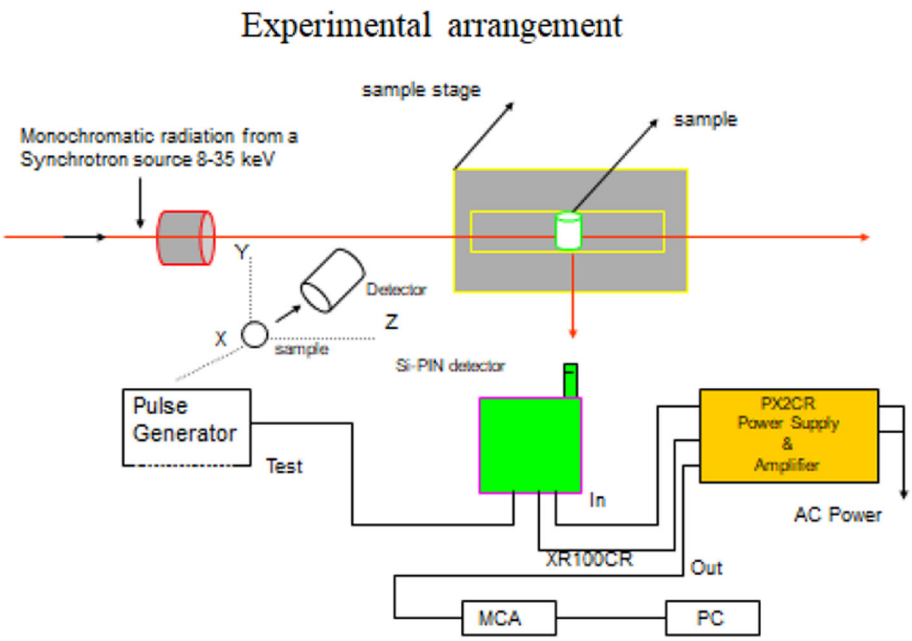

(a)

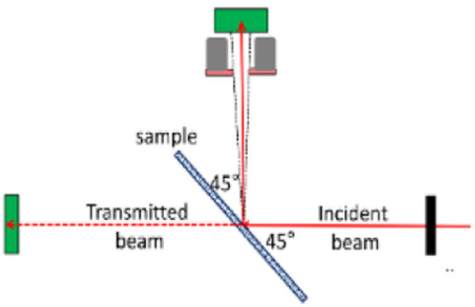

(b)

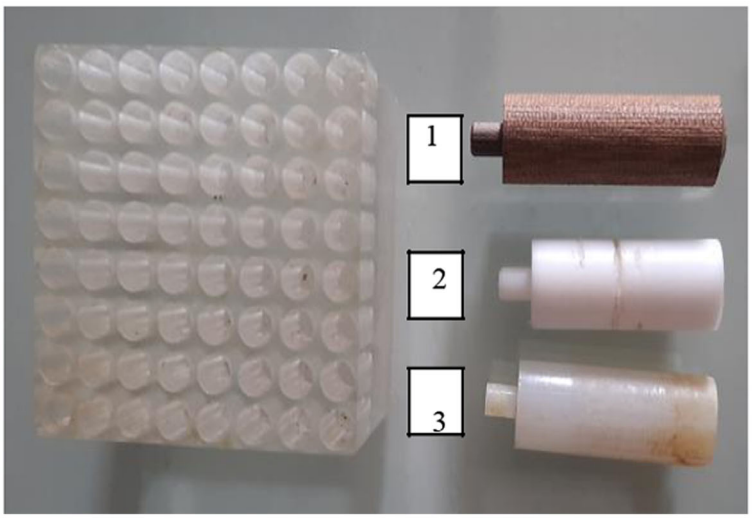

(c)

Fig. 1 **a** Experimental arrangement and the associated electronics used to detect the scattered radiation from the sample. **b** Experimental arrangement used to detect the scattered radiation from the sample in the reflection mode. **c** Physical dimension of the test phantom and few materials used with different dimensions suitable for the experimental study (1. Bakelite 2. Polyethylene 3. PMMA). **d** Electronics associated with the Si-PIN X-ray detector used

Fig. 1 continued

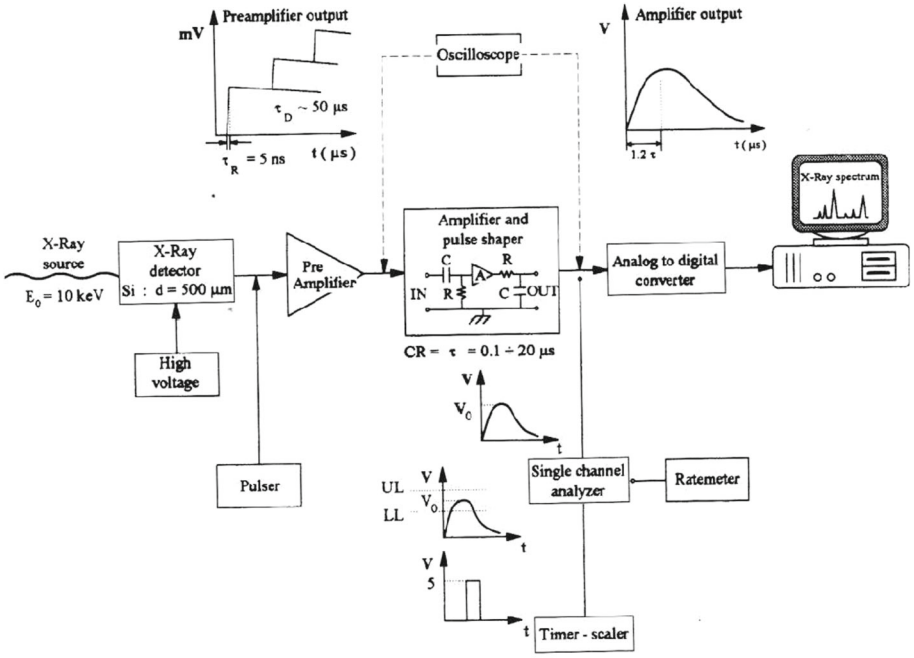

(d)

Table 1 Total attenuation (cm^2/g) for the incoming photons (10^8) with 5 mm thickness

Energy (keV)	Water	PMMA	Polyethylene	Bakelite	Muscle	Bone
10	26.5	16.8	10.45	14.2	27	100
15	8.35	5.5	3.75	4.75	8.5	31.65
20	4.05	2.85	2.16	2.535	4.15	14.15
30	1.88	1.5	1.355	1.405	1.9	4.9
40	1.34	1.175	1.135	1.12	1.345	2.6

Table 2 Compton attenuation coefficient values used at different energies

Energy (keV)	Water	PMMA	Polyethylene	Bakelite	Muscle	Bone
10	0.155	0.151	0.167	0.147	5.000	19.5
15	0.170	0.166	0.182	0.162	1.400	6.0
20	0.177	0.174	0.189	0.170	0.560	2.53
30	0.183	0.179	0.193	0.175	0.152	0.74
40	0.183	0.179	0.191	0.175	0.060	0.304

2.2.2 Estimation of transmission and Compton scattered photons for $(\Delta x)^2$, for the bounded area ABCD

The number of Compton photons scattered at an angle of 90° through the matrix for $(\Delta x)^2$ is estimated using Eqs. (2) and (3). The test phantom has 8×8 cylindrical holes of 4 mm diameter and 10 mm depth, orthogonal to the surface. The holes can be filled by liquids, mixtures, metals or left void. The 4π geometry and test phantom with 8×8 cylindrical holes are used [$1/4\pi\ 2e^2\ n^3$, for $n = 8$]. The physical dimension of the phantom is shown as an inset in Fig. 1c and also the cylindrical samples of other materials.

$$N_c = N_0 * 1.074 * 10^{-5}(\mu/\rho)_1^c \rho_1/(\mu/\rho)_0 \rho_0 \tag{2}$$

$$N_c = N_0 * 1.074 * 10^{-5}(\mu/\rho)_0^c \rho_1/(\mu/\rho)_0 = 2.86 * 10^{-3} * \left[\mu_{cw} - (\mu/\rho)_1^c \rho_1\right] \tag{3}$$

In the transmission mode, the number of transmitted photons thorough the matrix for $(\Delta x)^2$ and without matrix is estimated using Eq. (4).

$$N_{TM-T} = N_0 * 0.135 * \left[1 - 1.105e^{-0.266(\mu/\rho)_1 \rho_1}\right] \tag{4}$$

Table 3 The contribution of transmitted, Compton and fluorescence photons

Energy (kev)	Compton photons	Fluorescence photons	Bounded area	Interacted Compton photons in a bounded area: ABCD	Compton photons detected at a solid angle of 6.25×10^{-4}	Compton photons at 90^0
Water						
10	3.12E-04	9.95E-06	3.00E-04	8.68E-06	5.43E-09	1.68E-20
15	2.36E + 04	7.85E + 03	1.58E + 04	1.59E + 03	0.99	0.000235
20	1.74E + 06	1.02E + 06	7.15E + 05	1.55E + 05	97	1.68
30	1.53E + 07	1.21E + 07	3.12E + 06	1.51E + 06	941	144
40	2.62E + 07	2.05E + 07	5.65E + 06	3.82E + 06	2388	625
PMMA						
10	5.05E + 05	0.42	4.63	0.206	0	6.51E-12
15	4.08E + 06	1.79E + 05	2.28E + 05	3.41E + 04	21	0.087
20	5.78E + 06	3.84E + 06	1.94E + 06	5.87E + 05	366	21
30	2.23E + 07	1.84E + 07	3.88E + 06	2.29E + 06	1435	320
40	3.08E + 07	2.46E + 07	6.26E + 06	4.72E + 06	2953	912
Polyethylene						
10	2.89E + 03	4.55E + 02	2.44E + 03	1.92E + 02	0.12	3.49E-06
15	2.35E + 06	1.23E + 06	1.12E + 06	2.69E + 05	168	4
20	1.15E + 07	8.20E + 06	3.33E + 06	1.44E + 06	901	104
30	2.57E + 07	2.16E + 07	4.18E + 06	2.95E + 06	1845	476
40	3.21E + 07	2.57E + 07	6.42E + 06	5.34E + 06	3343	1075
Bakelite						
10	6.8E + 01	7.38	61	3.11	0.002	1.32E-09
15	8.65E + 05	4.10E + 05	4.54E + 05	7.67E + 04	48	0.42
20	7.92E + 06	5.43E + 06	2.49E + 06	8.28E + 04	517	41
30	2.45E + 07	2.04E + 07	4.08E + 06	2.51E + 06	1574	386
40	3.26E + 07	2.61E + 07	6.47E + 06	5.01E + 06	3132	1022
Muscle						
10	0.0002	5.74E-06	0.0002	5.11E-06	3.19E-09	6E-21
15	2.03E + 04	6.658E + 03	1.36E + 04	1.33E + 03	0.84	0.0002
20	2.57E + 06	9.20E + 05	6.55E + 06	1.37E + 05	86	1.35
30	3.49E + 06	1.18E + 07	7.08E + 06	1.45E + 06	910	136
40	2.60E + 07	2.04E + 07	8.63E + 06	3.75E + 06	2345	611
Bone						
10	3.72E-36	8.26E-41	3.72E-36	2.58E-38	1.61E-41	6E-85
15	1.8E-06	5.94E-08	1.74E-06	4.24E-08	2.65E-11	4.76E-25
20	72	15	56	3.21E + 03	0.002	1.44E-09
30	7.44E + 05	4.39E + 05	3.05E + 05	5.28E + 04	33	0.246
40	7.42E + 06	5.14E + 06	2.28E + 06	7.48E + 05	468	35

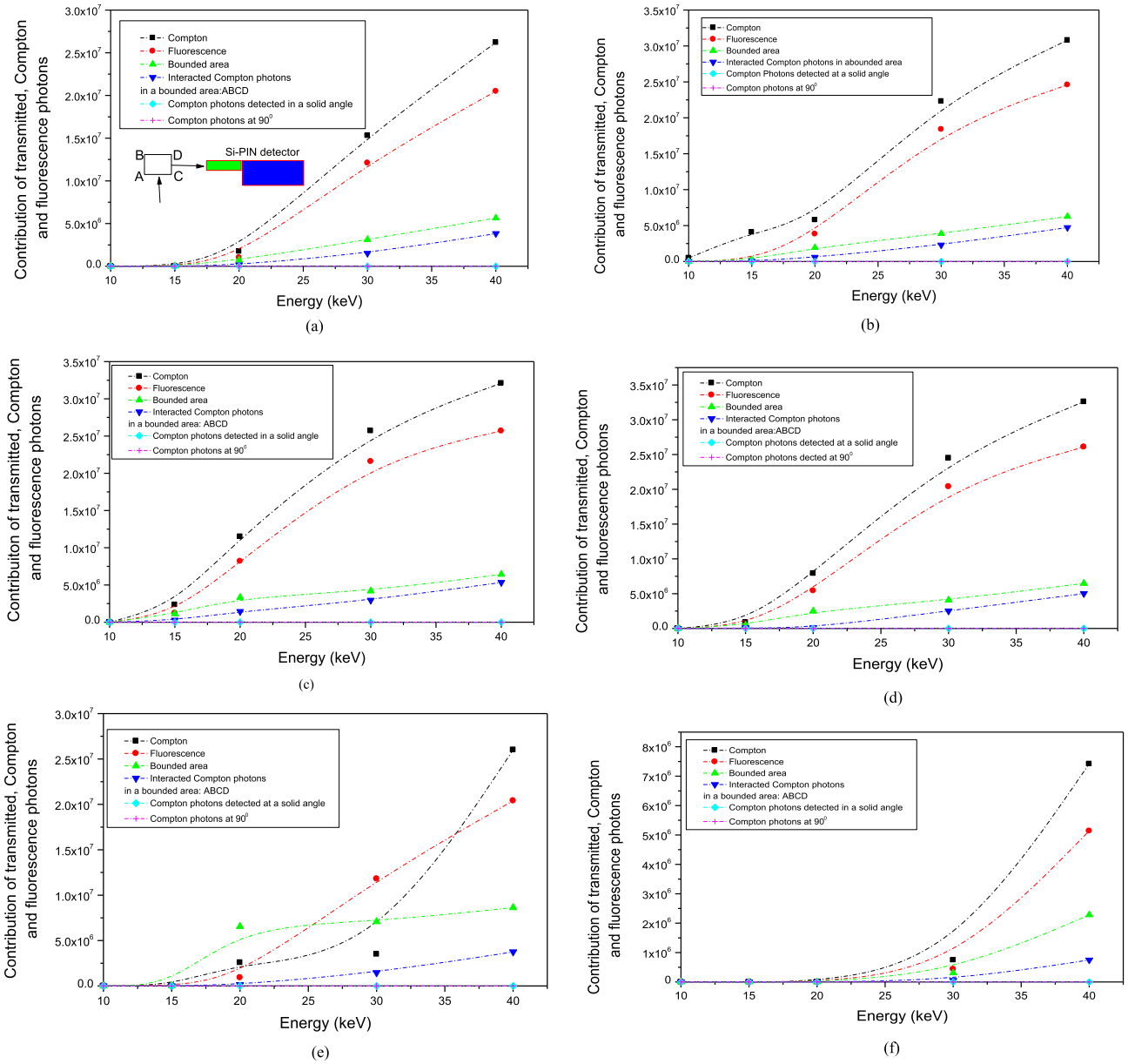

Fig. 2 a–f Estimation of photons in the energy region from 10 to 40 keV for Water, PMMA, Polyethylene, Bakelite, Muscle and Bone

where c_1, $(\mu/\rho)_1$ and ρ_1 are the concentration, the mass attenuation coefficient and the density of the material "1" and the matrix, respectively. The contribution of the fluorescence photons is assessed at an angle of 90° through the matrix for $(\Delta x)^2$ with inclusion of 1% of iodine to water using the following Eq. (5).

$$N_{fl} = N_0 * 2.94 * 10^{-5} \left[\frac{\mu_0 (1 - c_1) + \mu_1 c_1}{\mu_0^2} \right] \mu_{ph} \, . \, c_1 \, e^{-\mu(E_{fl})/\mu_0} \tag{5}$$

It considers the collimation and energy-dependent absorption of the detector sensor. The last term in Eq. (5) is the self-absorption correction term above the sub-volume of ABCD. Total attenuation for the incoming photons and Compton attenuation coefficients used at different energies are presented in Tables 1 and 2.

3 Results and discussion

The contribution of transmitted, Compton and fluorescence photons evaluated using simple approximations is presented in Table 3. Input values are assessed with the use of Eqs. (1)–(5). The measurements were continued by acquiring the spectra, until reaches less

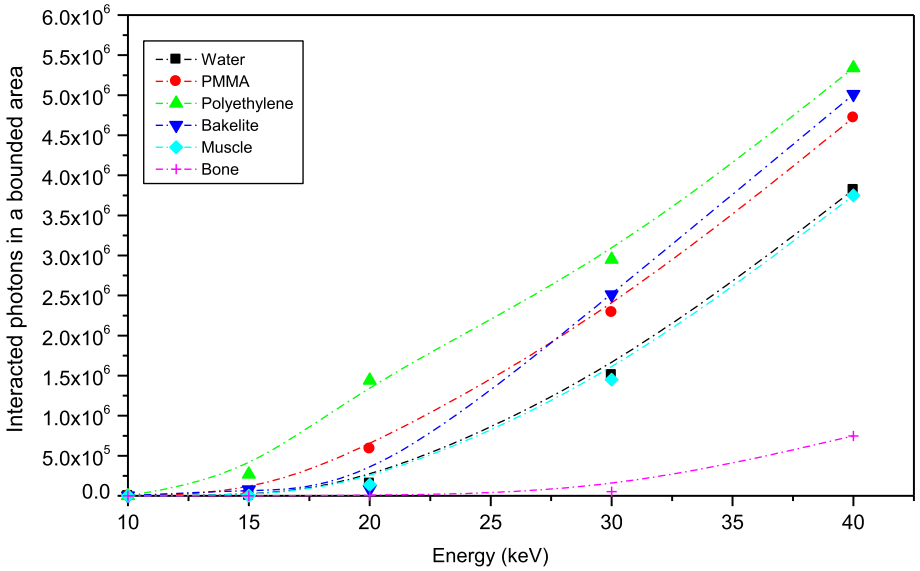

Fig. 3 Number of Compton photons interacted in Water, PMMA, Polyethylene, Bakelite, Muscle and Bone

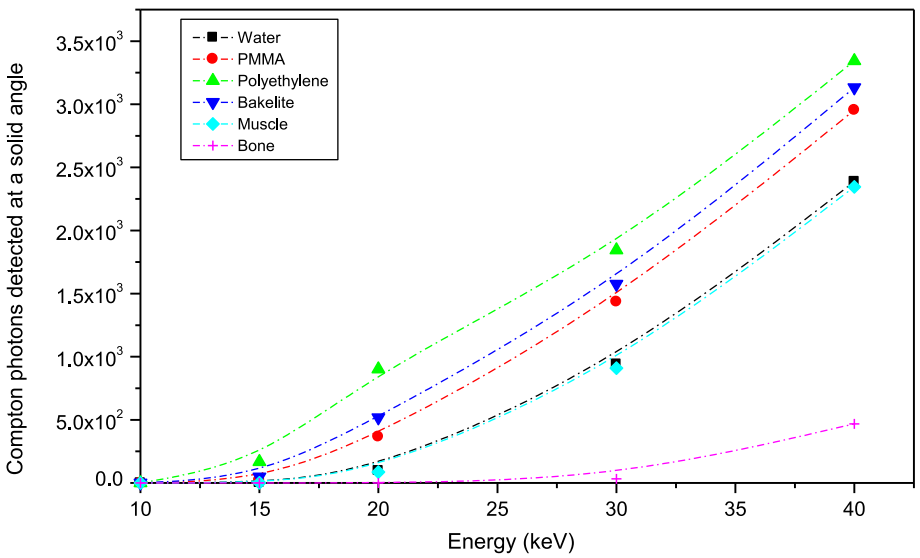

Fig. 4 Estimation of Compton scattered photons detected at a solid angle of 6.25×10^{-4} along line AC, from Water, PMMA, Polyethylene, Bakelite, Muscle and Bone

uncertainty for less than 1%. The calculations are obtained by assuming a perfectly monochromatic beam. Energy and thickness have been varied, for fixed incident photons. Theoretical attenuation coefficient calculations are performed with the use of XCOM [26], and the generated values are used for all the samples. The individual contributions of transmitted, Compton and fluorescence photons for a small volume, in the direction of θ from the incident beam, are estimated using the collimators attached to the detector in the experimental setup. The results are compared with the theoretical estimates based on simple approximations. Experimental results with a test phantom provided the optimum choice of energy. The estimated number of photons in the area bounded by ABCD and the number of photons interact due to Compton are displayed in Fig. 2a–f in the energy region 10–40 keV, for Water, PMMA, Polyethylene, Bakelite, Muscle and Bone. The number of Compton photons interacted estimated in Water, PMMA, Polyethylene, Bakelite, Muscle and Bone is displayed in Fig. 3. Figure 4 shows the estimation of Compton scattered photons for a given solid angle, and Fig. 5 shows the Compton photons at 90° for maximum attenuation.

Figures 6 and 7 show the total geometrical efficiency at an angle of 45° and 90° and with increase in the detector collimator length with fixed diameter. The geometrical efficiency can be maximized by using small sample detector and sample source distances. Here, the geometrical efficiency describes the interaction volume, which is the intersection of two volumes, i.e., the volume subtended by the incident X-ray beam and the volume subtended by the detector solid angle. The scattered spectrum is dominated by those of the polarized X-ray photons, which are incoherently scattered by the sample into the detector. The width of the distribution of the incoherently scattered photons increases with increasing opening angle of the collimators in front of the detector and X-ray source. The background in which the characteristic X-rays of the sample are registered in the pulse height distribution is due to the photons which are multiply scattered mainly in the investigated volume. Therefore, it is important to design the collimators in front of the

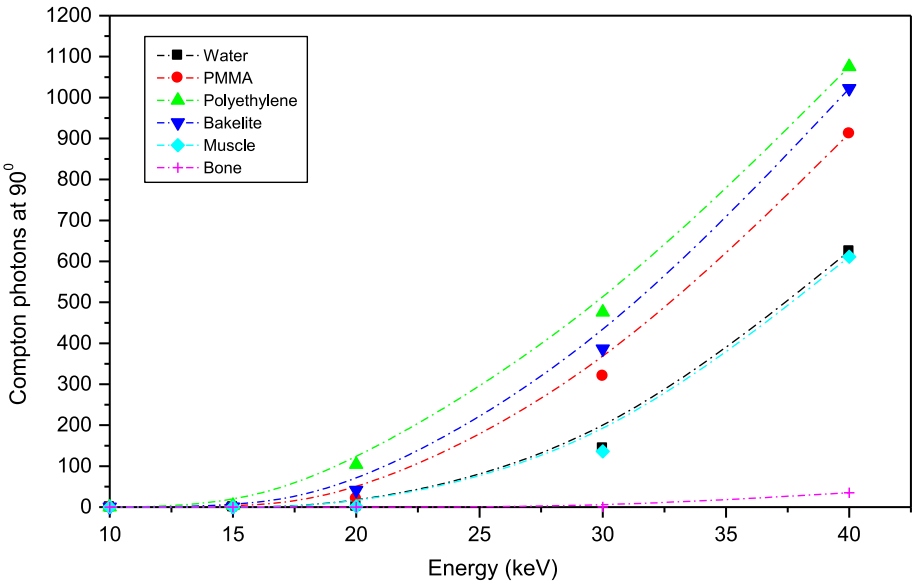

Fig. 5 The number of Compton photons detected at 90° for maximum attenuation, for Water, PMMA, Polyethylene, Bakelite, Muscle and Bone

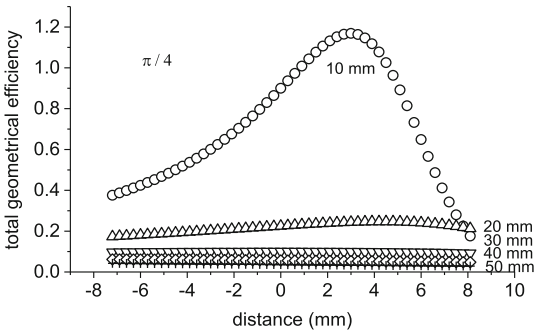

Fig. 6 Total geometrical efficiency at an angle of 45°

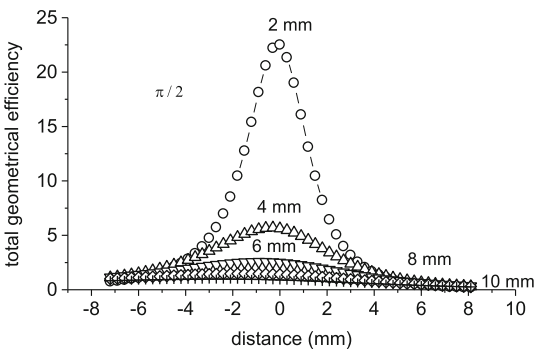

Fig. 7 Total geometrical efficiency at an angle of 90°

detector and the radiation source in order to improve the geometrical efficiency. The geometrical efficiency reaches to a maximum value and considerable deviation from the central position with increasing the length of the collimator toward the detector at an angle of 45°. However, for the 90° geometry, the total geometrical efficiency is higher and increases with decrease in the length of the collimator. The variation of the total geometrical efficiency from the central position of the sample is symmetric. Various combinations of collimator sizes, length and diameter, attached to the detector, allowed us to optimize the experimental parameters and optimization of geometrical effects, based on simple approximations. An analysis of the above parameters and their importance for various potential applications are thoroughly discussed [27].

The detector efficiency is considerably higher at lower photon energies (the detector efficiency is approximately 90% at 10 keV and 2% at 40 keV). The number of X-rays that reach the detector at a given angle depends not only on the scattering properties of the material at the center of the sample but also on the scattering and absorption properties of the material surrounding the center. Figures 6 and 7 suggest that at the experimentally measured angle (90°), most of the scattered events are due to Compton scattering and that a large percentage of these events are singularly scattered. The recorded events largely come from the small volume element of the sample corresponding to the point of intersection of the collimated source and detector axis.

The total number of scattered events recorded is quite high in the experimental study. This is because we were able to integrate all the events that were scattered into a small angle range $\theta \pm \Delta\theta$, because in the experimental study, the detector has a small finite area and because of that the total numbers of recorded scattered photons are high. The contribution of geometrical uncertainty is considerably varied with an angular interval of 1°, symmetrically situated around the centroid of the photopeak. The fluorescent signal is efficiently detected by suppressing inelastically scattered background. This provides an opportunity of selecting the optimum energies and geometrical arrangements for the source and detection system for the application of transmission and scattered radiation based on imaging. The relative uncertainty in theoretical estimates based on simple approximations is about 1–2%, which includes the input parameters. These are the initial results, which show the potential of using this procedure for further studies.

4 Conclusion

We have performed the experiments at various energies, to know the optimum energy, suitable for the detection of maximum number of transmitted, Compton and fluorescence photons, from the materials, routinely used as test phantoms. This way, the use of test phantom, will provide the assessment of contrast, to run the experiments further, to improve the quality of the image. The study, allowed us to optimize the experimental parameters and optimization of geometrical effects, based on simple approximations. The analytical studies with synchrotron X-rays have stimulated theoretical and experimental research in many areas, like material science-based X-ray imaging, for example, art and archeometry, X-ray fluorescence, X-ray diffraction, Compton profile methods and others. We have plans to extend the present study to lower energy region covering from 8 to 12 keV synchrotron X-rays.

Acknowledgements One of the authors (DVR) undertook part of this work with a financial assistance from ICTP-Elettra users program, Trieste, Italy, and science-based applications to Engineering, Physics Division, Universita di Roma "La Sapienza," Italy, as visiting professor, associating with Prof. G.E. Gigante. Further with a support from, Department of Bio-System Engineering, Yamagata University, Yonezawa 992-8510, Japan, and Kitasato University, Kitasato, Japan.

Author contributions D.V.Rao, G.E. Gigante and R. Cesareo helped in conceptualization; D.V.Rao helped in methodology; D.V.Rao and A.Brunetti. worked in software; D.V.Rao and A.Brunetti. helped in validation; N. Schiavon, T.Akatsuka, T.Yuasa and T.Takeda helped in formal analysis; D.V.Rao. helped in investigation; G.E.Gigante and R.Cesareo. helped in resources; D.V.Rao helped in data curation; D.V.Rao and G.E. Gigante. contributed to writing—original draft preparation; D.V.Rao and A. Brunetti. contributed to writing—review and editing; R.Cesareo. helped in visualization; G.E.Gigante. worked in supervision; G.E.Gigante. worked in project administration and D.V.Rao and G.E.Gigante. helped in funding acquisition.

Funding This research received no external funding.

Data Availability Statement This article has no associated data generated. The manuscript has associated data in a data repository.

Declarations

Conflict of interests The authors have nothing to disclose.

References

1. J.H. Hubbell, Photon mass attenuation and mass energy-absorption coefficients for H, C, N, O, Ar, and seven mixtures from 0.1 keV to 20 MeV. Radiat. Res. **70**, 58–81 (1977)
2. J.H. Hubbell, Photon mass attenuation and energy-absorption coefficients from 1 KeV to 20 MeV. Int. J. Appl. Radiat. Isot. **33**, 1269–1290 (1982)
3. J.H. Hubbell, Review of photon interaction cross section data in the medical and biological context. Phys. Med. Biol. **44**, R1-22 (1999)
4. J.H. Hubbell, Review and history of photon cross section calculations. Phys. Med. Biol. **51**, R245-262 (2006)
5. S.M. Seltzer, Calculation of photon mass energy-transfer and mass energy-absorption coefficients. Radiat. Res. **136**, 147–170 (1993)
6. D.P. Jackson, D. Hawkes, X-ray attenuation coefficients for elements and mixtures. Phys. Rep. **70**, 169 (1981)
7. R. Cesareo, A.L. Hanson, G.E. Gigante, L.J. Pedraza, S.Q.G. Mahtaboally, Interaction of keV photons with matter and new applications. Phys. Rep. **213**, 117–178 (1992)
8. D.V. Rao, T. Yuasa, T. Akatsuka, G. Tromba, M.Z. Hasan, T. Takeda, Tomographic imaging based on scattered radiation from polyethylene using 10, 15, 20, 25 and 30 keV synchrotron X-rays with simple approximations. NIM B. **239**, 209–216 (2005)
9. D.V. Rao, R. Cesareo, A. Brunetti, G.E. Gigante, T. Akatsuka, T. Yuasa, X-ray transmission and Compton CT investigation of some gastropods from Sassari. Sardinia Italy IS & T **32**, 127–137 (2004)
10. D.V. Rao, T. Takeda, Y. Itai, T. Akatsuka, R. Cesareo, A. Brunetti, G.E. Gigante, X-ray scattering cross-sections for molecules, plastics, tissues and few biological materials. JTMT. **20**, 327–361 (2002)
11. D.V. Rao, T. Takeda, Y. Itai, T. Akatsuka, R. Cesareo, A. Brunetti, G.E. Gigante, Doppler broadening and its contribution to Compton energy-absorption cross-sections: an analysis of the Compton component in terms of mass-energy absorption coefficient. J. Phys. Chem. Ref. Data **31**(2002), 769–818 (2002)
12. R. Cesareo, S. Mascarenhas, New tomographic device based on the detection of fluorescent x-rays. NIMA. **277**(1989), 669–672 (1989)
13. R. Cesareo, S. Mascarenhas, S. Crestana, A. Castellano, New tomographic methods using X-ray tubes. NIMA. **299**, 440–443 (1990)
14. R. Cesareo, C.B. Cesare, A. Brunetti, B. Golosio, A. Castellano, A simple scanner for Compton tomography. NIM A. **487**, 188–192 (2002)
15. R. Cesareo, A. Brunetti, B. Golosio, R.T. Lopes, R.C. Barroso, A. Castellano, S. Quarta, Material analysis with a multiple X-ray tomography scanner using transmitted and scattered radiation. NIM A. **525**, 336–341 (2004)

16. R.D. Speller, J.A. Horrocks, Photon scattering- a new source of infromation in medicine and biology? Physics in medicine and biology. Phys. Med. Bio. **36**, 1–6 (1991)
17. G.J. Royle, R.D. Speller, Low angle X-ray scattering for bone analysis. Phys. Med. Bio. **36**, 383–389 (1991)
18. R.D. Speller, G.J. Royle, Tissue characterisation using low angle X-ray scattering. JXST. **3**, 77–84 (1992)
19. R.D. Speller, J.A. Horrocks, R. Lacey, X-ray scattering signatures for material identification. SPIE. **2092**, 366–377 (1993)
20. D.V. Rao, G.E. Gigante, R. Cesareo, Coherent and incoherent scattering of 42.75 and 47.24 keV X-ray photons scattered from Al, Cu, Y, Mo, Au and Pb. X-ray. Spectro. **24**, 172–176 (1995)
21. A. Brunetti, R. Cesareo, D.V. Rao, B. Golosio, Geometrical influence on Compton profile measurement for biological samples. NIM A **526**, 584–592 (2004)
22. L. Grodzins, Optimum energies for X-ray transmission tomography of small samples. NIM. **206**, 541–546 (1983)
23. L. Grodzins, Critical absorption tomography of small samples. NIM **206**, 547–552 (1983)
24. P. Spanne, X-ray energy optimisation in computed microtomography. Phys. Med. Biol. **34**, 679–690 (1989)
25. D.V. Rao, R. Cesareo, A. Brunetti, Computed tomography with image intensifier: imaging and characterization of materials. NIM A. **437**(1999), 141–151 (1999)
26. M. J. Berger, J. H. Hubbell, XCOM: Photon cross sections on a personal computer, NBS Internal Report (1987) NBSIR 87–3597
27. D.V. Rao, R. Cesareo, A. Brunetti, G.E. Gigante, T. Akatsuka, T. Takeda, Y. Itai, Geometrical efficiency, solid angle contribution and gradient for a triaxial system equipped with a fluorescent source and x-ray tube: an analysis to enhance the Compton scattered photons. X-Ray Spectrom. **33**, 87–100 (2004)